9

Atmospheric Pressure Plasma Jet Induced Graft-Polymerization for Flame Retardant Silk

Dheerawan Boonyawan
Chiang Mai University,
Thailand

1. Introduction

Improving the flame retardant property of textiles become necessary to minimize the fire hazard under many circumstances (Wichman, 2003). Since fire accidents cause injuries and fatalities and also devastate property, considerable efforts have been made to develop flame-retardant textiles. Silk is one of the most commonly used textiles for interior decoration, such as upholsteries, curtains, and beddings, for its luxurious appearance. It is therefore of primary significance to improve the flame retardant property of silk fabrics in which the safety regulations are concerned. Flame retardant fabrics are typically prepared by treating the fabrics chemically with flame retardant agents. Halogen-based flame retardant agent is one of the most efficient reduction of the fire hazard for fabrics. However, because of their corrosivity, the presence of dioxin, a carcinogen, and suspected smoke toxity by products, there are legislated regulations to restrict halogen-based flame-retarded textile products. The non-halogen-based flame retardants have subsequently been replaced. Phosphorous-based compounds are the most extensively used (H. Yang & C. Yang, 2005) (Gaan & Sun, 2007), (Wu & C. Yang, 2007), (Horrocks & Price, 2001). For natural fiber textiles, a number of studies focus on flame retardant property of cotton fabrics (Reddy *et al.*, 2005), (Wu & C. Yang, 2006), (Tsafack & Levalois-Grützmacher, 2006) and silk fabrics (Achwal *et al.*, 1987), (Kako & Katayama, 1995), (Guan *et al.*, 2009). It was shown that a high level of flame retardancy could be achieved when silk fabric was treated by a reaction mixture of urea and phosphoric acid through pad/dry process (Achwal *et al.*, 1987). However, the treated silk had limited laundering durability. The flame retardant agent under the commercial name "Pyrovatex CP" which is N-hydroxymethyl (3-dimethylphosphono) propionamide (HDPP) was applied to induce flame retandancy on silk (Kako & Katayama, 1995) and (Guan & G. Chen, 2006). This compound needs formaldehyde, which is one of human carcinogens, as the bonding agent. Recently, the use of formaldehyde-free flame retardant finishing process was developed (Guan & G. Chen, 2006). The treated silk shown improved flame reatadancy with limited laundering durability. Although varying degrees of flame retardancy were obtained, the durability is difficult to solve due to the water solubility of the agent. It is even more problematic when the textiles are from natural origins. The development of satisfactory, durable flame retardant silk is indeed challenging and the alternative eco-friendly processes have to be considered.

Plasma treatment is a potential technique to impart flame retardant properties to textiles. The reactive species in the plasma interact with the surface atoms or molecules and modify the surface properties without affecting bulk properties. Recently, it was reported that microwave plasma had been employed in the flame retardant finishing process (Tsafack & Levalois-Grützmacher, 2006a) and (Tsafack & Levalois-Grützmacher, 2006b). However, low pressure plasma systems need to operate under vacuum which, in turns, add the cost and complexity to the process. Atmospheric pressure plasma source is an alternative system. A few different designs have been developed and employed to modify the surface of materials (Cheng *et al.*, 2006), (Schafer *et al.*, 2008), (Guimin *et al.*, 2009) and (Osaki *et al.*, 2003). The system is promising to industrial application since the vacuum system is eliminated.

In this work (Chaiwong *et al.*, 2010) we utilized an atmospheric pressure plasma jet to graft phosphorus-based flame retardant agent onto silk. The treated silk fabrics were submitted to 45° flammability test. The incorporation of phosphorus was studied via quantum simulations and Energy-Dispersive X-ray spectroscopy (EDS). The durability of the treatment was evaluated.

2. The setup

2.1 The silk

Silk, which is derived from the silk moth *Bombyx mori*, has a heavy chain that consists mainly of glycine (44%) and alanine (30%) (Dhavalikar, 1962). Silk yarn is scoured (degummed) to remove sericin, a gummy deposit on silk fibers. The crystal structure of silk fibroin has been examined by several research groups using the constrained least-squares refinement (Takahashi *et al.*, 1999). The simplest model consistent with the X-ray scattering pattern is Gly-Ala or Ala-Gly. Although these structures were solved earlier (Tranter, 1953, 1956) and (Naganathan & Venkatesan, 1972) the Gly-Ala structure is polymorphic, indicating the flexibility and the potential of possible alternate structures.

Silk fabric (Grazie™) of a density 52.9 g/m^2 used in this study, has a warp density and a weft density of 129 and 99 per inch respectively. The air penetration resistance was 98.4 cm^3/cm^2·s indicating that the silk has high air resistance. The fabric was cut into 5 cm×17 cm samples which size fit to the flame spread test.

2.2 Plasma jet system

A self-made plasma jet system used is shown schematically in Fig. 2. The inner hollow electrode covered with a quartz tube was centred at the axis of the outer electrode. The inner electrode was connected to a 50 kHz, 0–10 kV voltage source whereas the outer electrode was grounded. High purity Ar was used as a plasma gas with adjustable flow rate from 2 to 10 standard litre per minute (slm). The gas flow was controlled by a gas flow controller. The operating voltage was set to 8 kV to keep constant input power to plasma.

The plasma jet was monitored by using a S2000 fibre optics spectrometer (Ocean Optics Inc, USA). The fiber optics probe was placed at right angle to the jet axis at a distance of 5 mm away. The emission spectrum of the plasma was collected at 0.3 nm resolution. The emission spectrum of the Ar plasma jet measured at the sample position which is 5 mm from the jet nozzle is shown in Fig. 3. It can be seen that the spectrum in the wavelength range of 250–

850 nm was dominated by excited argon (Ar I) peaks. In addition, reactive radical peaks including hydroxyl (OH) and atomic oxygen were found at 308.9 nm and 777.1 nm, respectively. Ambient species, such as N_2, were also observed. The presence of these radicals was undesirable since they might react with the surface of the samples. However, the emergence of these species could be controlled by the system parameters. For example, the OH band was drastically suppressed if the discharge voltage increased. The Ar flow rate was one of the parameters that affect the presence of radical species. It was found that excited N_2 peaks appeared more intense than OH radicals if the Ar flow rate was over 6 slm.

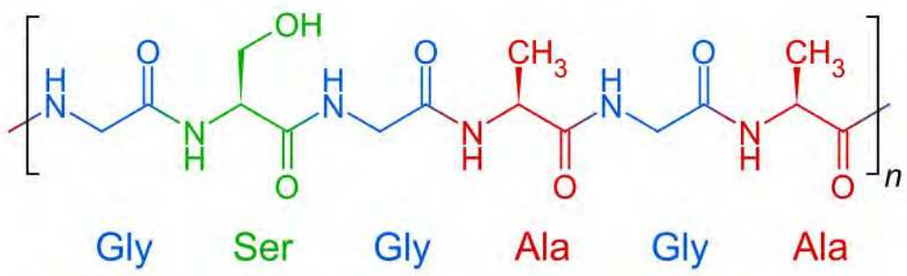

formula	code	Z	R factor	density /g.cm-3	space group	cell parameter					
						a/Å	b/Å	c/Å	α/°	β/°	γ/°
$C_6N_2O_3H_{14}$	AG	2	0.059	1.439	$P2_1$	5.28	11.81	5.51	90	101	90
$C_6N_2O_3H_{14}$	GA	4	0.045	1.549	$P2_12_12_1$	9.68	7.53	9.53	90	90	90

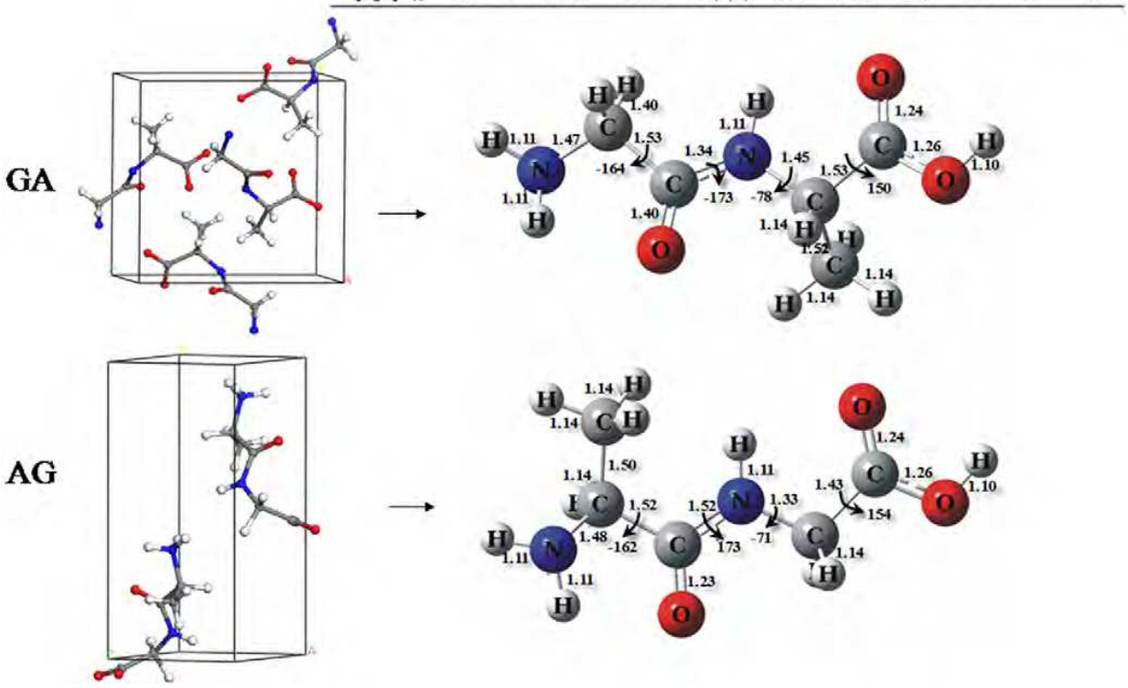

Fig. 1. The crystal structures of untreated GA and AG and corresponding cell parameters using single crystal X-ray diffraction technique (Sangprasert *et al.*, 2010).

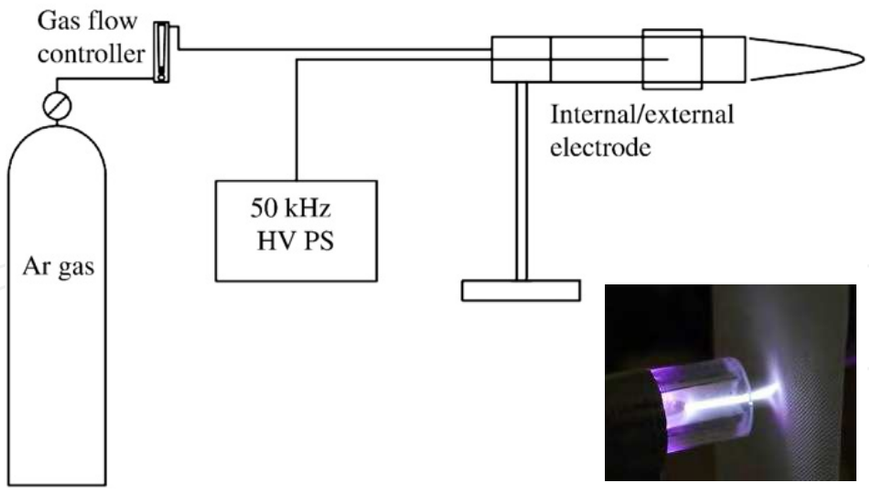

Fig. 2. Schematic view of self-made plasma jet system and the treatment (inset).

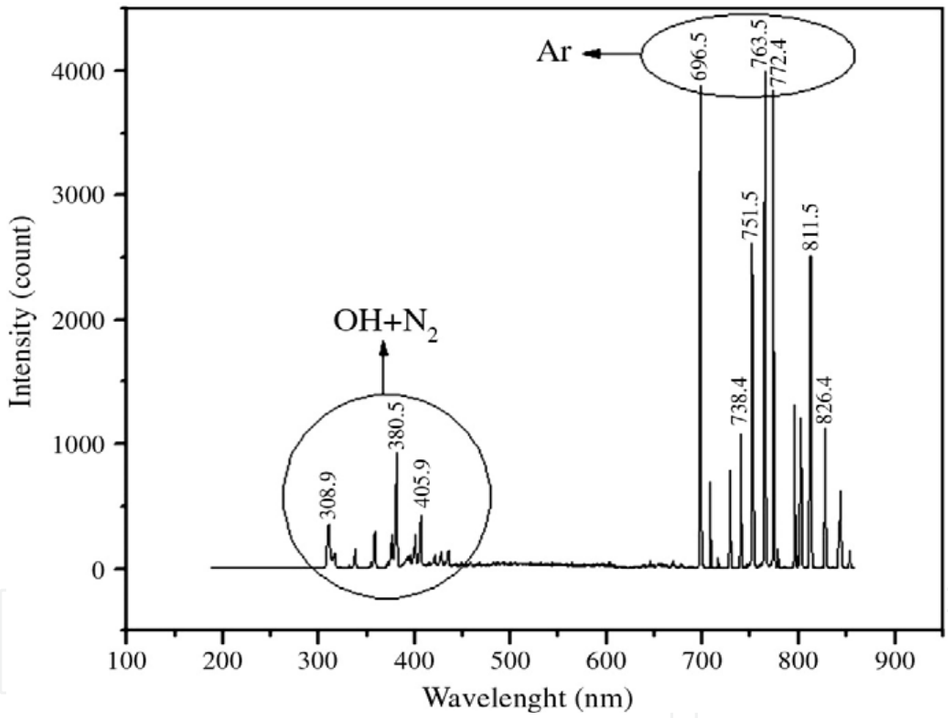

Fig. 3. Ar plasma emission spectrum at sample position from plasma jet, 6 slm flow.

2.3 The electron temperature

One important parameter to describe a plasma is its electron temperature, T_e. The plasma jet is one of a non-equilibrium plasma which electron temperature is a magnitude greater than the ion and the gas temperature. Determination of the electron temperature of our atmospheric plasma jet by optical emission spectroscopy (OES), the Boltzmann-plot method was applied. For this purpse a plot of ln ($I\lambda/gA$) versus E_k should result a straight line with a slope of $-1/T_e$. I_k is the intensity of the emitted light, λ_k is the wavelength, g_k is the statistical

weight, A_k is the transition probability, and E_k is the energy of the upper level. Table 1 shows the most intense Ar lines observed in the plasma and their characteristics.

Line	λ (nm)	Upper state (i)	Low state (j)	E_i (eV)	E_j (eV)	g_i	g_j	A_{ij} ($10^8 s^{-1}$)
Ar I	415.859	5p	4s	14.56	11.55	5	5	0.0140
Ar I	416.418	5p	4s	14.53	11.55	3	5	0.00288
Ar I	418.188	5p	4s	14.69	11.72	3	1	0.00561
Ar I	419.071	5p	4s	14.51	11.55	5	5	0.00280
Ar I	419.832	5p	4s	14.58	11.62	1	3	0.0257
Ar I	420.068	5p	4s	14.50	11.55	7	5	0.00967
Ar I	425.936	5p	4s	14.74	11.83	1	3	0.0398
Ar I	427.217	5p	4s	14.52	11.62	1	1	0.00797
Ar I	452.232	5p	4s	14.46	11.72	3	1	0.000898
Ar I	706.722	4p	4s	13.30	11.55	5	5	0.0380
Ar I	714.704	4p	4s	13.28	11.55	3	5	0.00625
Ar I	727.294	4p	4s	13.33	11.62	3	3	0.0183
Ar I	738.398	4p	4s	13.30	11.62	5	3	0.0847
Ar I	750.387	4p	4s	13.48	11.83	1	3	0.445
Ar I	751.465	4p	4s	13.27	11.62	1	3	0.402
Ar I	763.511	4p	4s	13.17	11.55	5	5	0.245
Ar I	794.818	4p	4s	13.28	11.72	3	1	0.186
Ar I	800.616	4p	4s	13.17	11.62	5	3	0.0490
Ar I	801.479	4p	4s	13.09	11.55	5	5	0.0928
Ar I	810.369	4p	4s	13.15	11.62	3	3	0.250
Ar I	811.531	4p	4s	13.08	11.55	7	5	0.331

Table 1. the most intense Ar lines observed in the plasma and their characteristics (NIST, 2009).

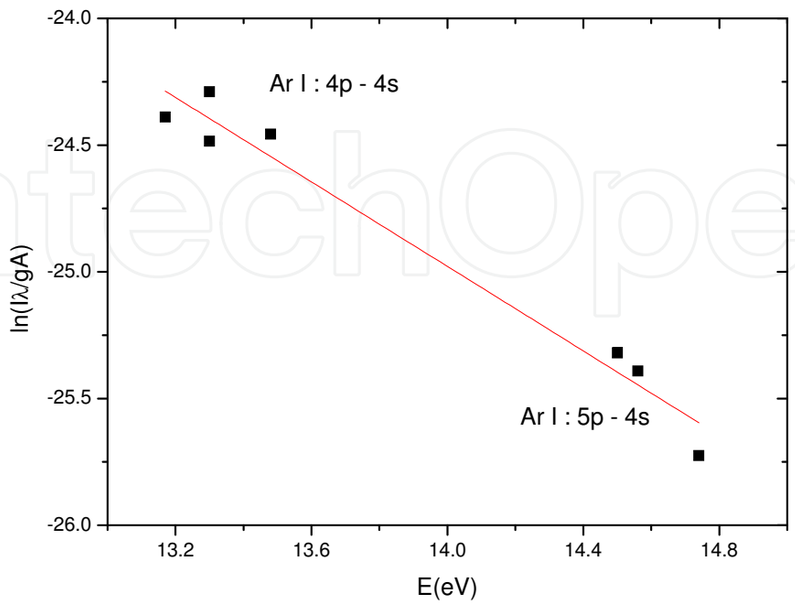

Fig. 4. Boltzman plot to determine the electron temperature of the plasma jet.

Atmospheric plasmas jet was generally in near-partial-local thermodynamic equilibrium (PLTE) (Griem, 1964). Thus, the distribution of atoms and ions in different excited states could be described by the Boltzmann distribution function, and the well-known method of Boltzmann-plot. From the OES in Fig.3, two groups of distribution points for Ar I transitions: 4p–4s and 5p–4s have been observed. The electron temperature has derived from fitting procedure for all of these points. The slope revealed the electron temperature of 1.3 eV. The electron temperature of this setup varied from 1.0-1.3 eV depends on the argon flow rate. The presence of Ar II lines has not shown since these lines are commonly observed in low-pressure plasmas but not in high-pressure discharges. In a DC microplasma plasma jet (Sismanoglu *et al*., 2009), reported the presence of Ar II lines with a hollow anode configuration.

2.4 Treatment of the silk

Plasma-Surface Interactions

Like others plasma sources, many fundamental processes take place at the plasma-substrate interface as shown in Table 2. The surface is reached by fast electrons, ions, and free radicals, combined with the continued electromagnetic radiation emission in the UV-vis spectrum enhancing chemical-physical reactions. The minimum energy required to remove an electron from the highest filled level in the FERMI distribution of a solid into vacuum (to a point immediately outside the solid surface) is given by the work function eφ, with φ being the electron emission potential. The energy can be provided thermally (phonons, kBT), photons (ħω) or from the internal potential energy or kinetic energy of atoms and ions or metastable excited states.

Reactions	Description
AB + C(solid) → A + BC(gas)	Etching
AB(gas) + C(solid) → A(gas) + BC(solid)	Deposition
$e^- + A^+ \rightarrow A$	Recombination
$A^* \rightarrow A$	De-excitation
$A^* \rightarrow A + e^-$ (from surface)	Secondary Emission
A^* (fast) → $A + e^-$ (from surface)	Secondary Emission

Table 2. Plasma-surface reactions (adapted from Braithwaite, 2000).

Presence and concentration of plasma active species is strongly dictated by the operational parameters of the plasma discharge used. Since electrons initialize ionization, changes of the electron gas (density, temperature, electron energy distribution function, (EEDF)) strongly influence the formation, the concentration and chemical reaction rate of reactive species and the intensities of the different wavelength emissions. The electron gas parameters in turn depend on the operational parameters of the plasma such as power, excitation frequency, gas flow and pressure.

Electrons

It is known that plasma electrons are not mono energetic. This is important as the rates of plasma-chemical reactions depend on the number of electrons with energy equal or higher

to the reaction-specific threshold. The probability density for an electron having a specific energy ε can be described by means of the electron energy density function. The EEDF strongly depends on the electric field and the gas composition in a plasma and often is very far from being a real equilibrium distribution. Due to the various assumptions made in the quasi-equilibrium Maxwell-Boltzmann approximation, the EEDF of non- local thermodynamic equilibrium (LTE) plasmas is often better approximated by the Druyvesteyn distribution function.

$$f(\varepsilon) = 1.04\langle\varepsilon\rangle^{-3/2}\,\varepsilon^{1/2}\exp\left(-\frac{0.55\varepsilon^2}{\langle\varepsilon^2\rangle}\right)$$

As can be seen in Fig. 5, the Druyvesteyn distribution function is characterized by a shift toward higher electron energies.

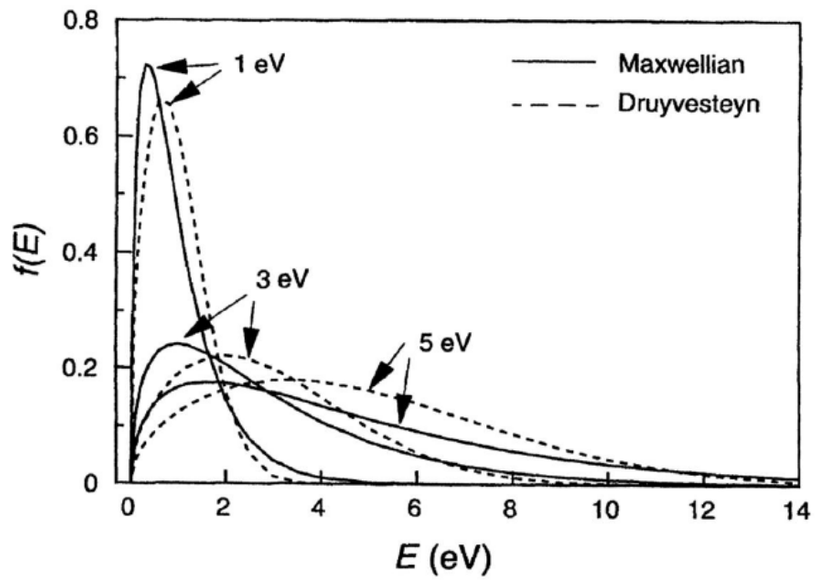

Fig. 5. Electron energy distributions according to Druyvesteyn and Maxwell. The numbers indicate the average electron energy for each distribution (Grill, 1994).

Both energy distributions however, regardless of the adopted approximation, show an important fact: While the majority of the electrons in non-LTE plasma have a low electron energy range (0.5-4 eV), there exist a very small but significant number of electrons characterized by a depleted high-energy tail region (8-15 eV). Though small in numbers, these electrons significantly influence the overall reaction rates in plasma, contributing to reactions, requiring a specific energy threshold value. Most of the electrons in this kind of plasma have energies high enough to dissociate almost all chemical bonds as shown in Table 3.

Ions

As ionization rates of ions in non thermal plasma are much lower than those for molecular dissociation, radical species density can be orders of magnitude higher than that of ions.

Therefore, plasma chemistry was inferred of being mainly governed by radical reactions, or by photochemical means. Due to the often high kinetic energy they gain in the plasma sheath, ions are considered to substantially contribute to plasma-chemical kinetics (Becker *et al.*, 2004). Ion formation reactions have been regularly illustrated by excitation, ionization, dissociation, and further electron impact reactions, like dissociative ionization or dissociative attachment by plasma electrons. Consequently, the various loss channels of positive and negative ions are as listed in Table 4.

Bond type	Bond energy ($kJmol^{-1}$)	Bond energy (eV)
C-H	411	4.25
C-C	346	3.56
C-N	276	2.86
C-O	358	3.70
C-S	272	2.80
C=C	602	6.23
C=O	724	7.50
C≡C	835	8.65
N-H	385	3.99
O-H	456	4.73

Table 3. Dissociation energies of organic compounds (Mathew *et al.*, 2008).

Reactions	Description
$e^- + AB^+ \rightarrow (AB)^* \rightarrow A + B^*$	Dissociative Electron-Ion Recombination
$e^- + A^+ \rightarrow A^* \rightarrow A + \hbar\omega$	Radiative Electron-Ion Recombination
$2\,e^- + A^+ \rightarrow A^* + e^-$	Trimolecular Electron-Ion Recombination
$A^- + B^+ \rightarrow A + B^*$	Bimolecular Ion-Ion Recombination
$A^- + B^+ + M \rightarrow A + B + M$	Trimolecular Ion-Ion Recombination
$e^- + M \rightarrow (M^-)^* \rightarrow M^- + \hbar\omega$	Radiative Electron Attachment
$e^- + A + B \rightarrow A^- + B$	Trimolecular Electron Attachment
$A^+ + B \rightarrow A + B^+$	Ion-Atom Charge Transfer
$A^+ + 2\,A \rightarrow A_2^+ + A$	Ion Conversion
$e^- + AB \rightarrow A^+ + B^- + e^-$	Polar Dissociation
$e^- + A^- \rightarrow A + 2\,e^-$	Electron Attachment

Table 4. Loss reactions of positive and negative ions in plasma (Fridman, 2008).

Ion chemistry of atmospheric plasmas is said to be rich. One example is the ion-induced formation of dangling bonds, acting as chemisorption sites for alkyl or any other free radicals (Von Keudell & Jacob, 2004). Their formation from impinging energetic ions has been recently demonstrated by particle beam experiments (Kylian *et al.*, 2009) and (Raballand *et al.*, 2008). Fig. 6 demonstrates surface active sites can be attacked by oxygen species (atomic or molecular oxygen) which leads either to fast passivation of the surface defect structure giving rise to various oxygen functional groups. Or a gradual volatilization occurs, namely of H_2O, $^{\cdot}OH$, CO and CO_2, which diffuse from the bulk to the surface and desorb (Coburn & Winters, 1979).

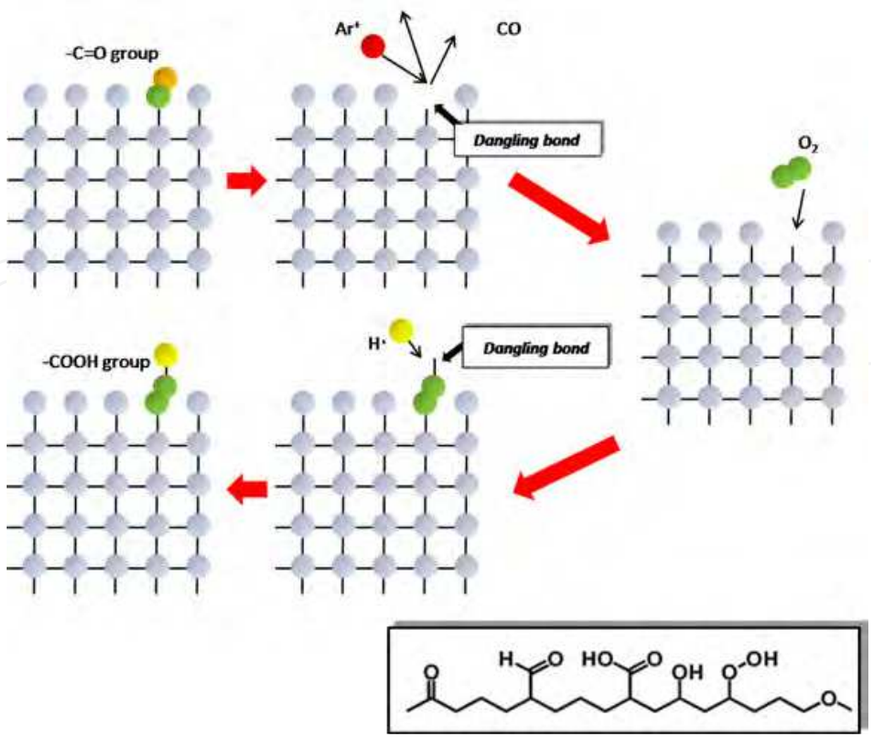

Fig. 6. Radicals (ions) in plasma interact with adjacent solid surface perform a functional surface. (Grzegorzewski, 2011)

Although the generation of dangling bonds is a strongly endothermic process, the high ion kinetic energy is usually sufficient for homolytical cleaving chemical bonds (Table 3). For atmospheric plasma jet, ion energy up to hundred eV is possibly obtained by a few hundred-negatively biased of the substrate.

Photons

At high pressures, single-collision conditions do not longer prevail. Beyond binary collisions, three-body interactions take place, leading to the formation of excimers. Rare gas excimer formation usually proceeds via electron-impact ionization or directly by metastable rare gas atom excitation. In either case, the initial step is a three-body collision process in which two ground state atoms interact with an excited state atom (metastable state or resonance, Table 5). Efficient excimer formation requires both a sufficiently large number of electrons with energies above the threshold for the metastable formation (or ionization), and a pressure that is high enough to have a sufficiently high rate of three-body collisions (Kurunczi *et al*., 2001). In case of Ar, the minimum energy needed to form a metastable Ar atom by electron impact on ground-state Ar is about 12 eV.

It is due to this unique environment that non-LTE plasmas are not only able to increase the efficiency of traditional chemical processes. They offer as well alternative approaches to in conventional chemical synthesis otherwise inaccessible reaction pathways, often by changing the symmetry of the molecule's electronic configuration. The initiation of novel reaction channels at moderate bulk temperatures might lead to new transient and secondary products, which is an often highly desired and already exploited result of plasma treatment.

However, the generation of high chemically active species harbors as well the risk of not only uncontrollable but as well undesired plasma-chemical synthesis. A thorough knowledge of plasma reaction chemistry therefore is mandatory for any industrial application.

Reaction	Description
$e^- + X \rightarrow X^+ + 2e^-$ $X^+ + 2\,X \rightarrow X_2^+ + X$ $X_2^+ + e^- \rightarrow X^* + X$ $X^* + 2\,X \rightarrow X_2^* + X$	Electron-impact ionization
$e^- + X \rightarrow e^- + X^*$ $X^* + 2\,X \rightarrow X_2^* + X$	Electron-impact excitation
$X_2^* \rightarrow 2\,X + \hbar\omega$	Radiative decay

Table 5. Rare gas excimer formation

2.5 Flame retardant compound grafting

Plasma induced grafting is the two-step process. Prior grafting, the free radicals formation by using inert gas plasma is included. The active sites for further reaction are generated on the surface by the subsequent plasma species as mentioned above. In this case, Ar plasma jet was initiated at 8 kV with 4 slm. These parameters were kept constant for all of the Ar treatments. The sample surfaces was pre-activate for 5 min with Ar plasma. The distance between the nozzle and the sample was set at 5 mm. After Ar pre-treatment, the samples were immersed in the finishing solution of PBS for 10 s and air dried at 60 °C for 10 min. Graft polymerization was performed with Ar plasma for 5 min. These samples were designated as Ar-PBS-Ar silk. The samples were finally immersed in ethanol to remove the residual un-grafted molecules and dried in air at room temperature. For comparison, samples without Ar pre-treatment, directly immersed in the PBS solution were prepared and designated as PBS silk.

2.6 The test

2.6.1 Washing stability testing

To evaluate the laundering durability of the flame retardancy, the samples were washed according to TIS-121 (3–1975) in an 1 g/L solution of commercial non-ionic detergent and tap water and at 35 °C for 30 min. The samples were air dried and stored in a desiccator until required.

2.6.2 Surface and chemical composition analysis

Scanning electron microscopy (SEM) and energy dispersive x-ray spectroscopy (EDS) were used to examine the surface of the samples and well as the chemical composition before and after the washing process. The SEM used in this work was a JSM 633S (Jeol, Japan) equipped with EDS. Additionally, Fourier transform infrared spectroscopy (FTIR) was done to extract the chemical bonding on the surface of the samples. The IR spectra were obtained by using a Nicolet 6700 FTIR spectrophotometer (Bruker, Germany) operated in attenuated total reflectance (ATR) mode. The spectra were collected by averaging 64 scans at a resolution of 4 cm^{-1} from 400–4000 cm^{-1}.

By comparing the SEM micrographs of the PBS silk (Fig. 7(a)) and the washed Ar-PBS-Ar silk Fig. 7(b), the grafting of PBS can be observed. As shown in Fig. 7(a), PBS particles deposited locally on the knot of the silk yarn. The surface topography along the yarn was relatively smooth. In contrast, the yarn of the washed Ar-PBS-Ar silk was rough and uniformly covered with the PBS particles. It is evident that the durable flame retardant property of silk can be obtained via Ar plasma grafting.

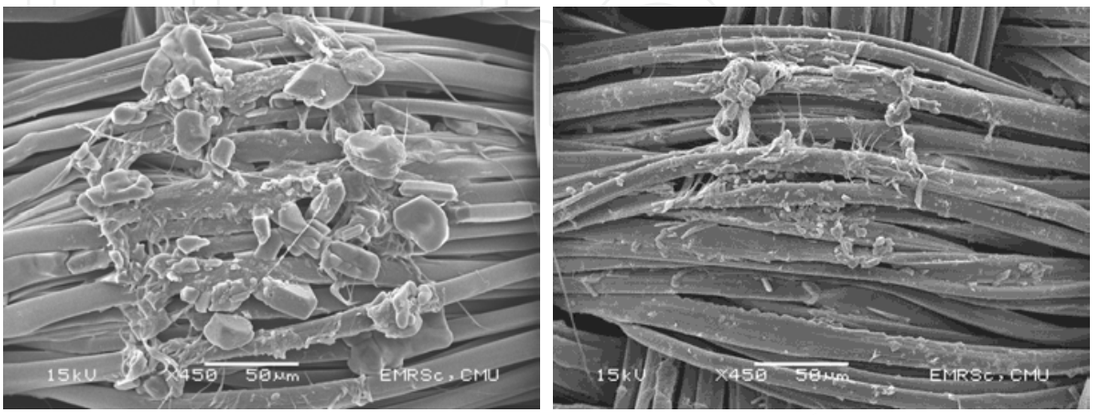

a b

Fig. 7. SEM micrograph of; a) PBS silk and; b) washed Ar-PBS-Ar silk

Fig. 8 shows the EDS spectrum obtained from the deposit on the yarn knot of the PBS silk. The spectrum showed evidence of phosphorus arising from PBS compound. Peaks of silk compositions, such as N, C, and O, were revealed. Calcium is one of the fingerprints of natural silk. Quantitative analysis of phosphorus content in the samples was done by means of EDS. The phosphorus content in the Ar-PBS-Ar was found to be 11% weight higher than that in the PBS silk, whose phosphorus content was 7% weight. This high level of phosphorus content in the Ar-PBS-Ar silk remained constant after the washing process. The results clearly indicate that in order to achieve durable flame retardant property, graft polymerization is necessary. The Ar plasma jet used in this work allowed us to bind covalently the flame retardant compound to the silk fabric. One can say that after the washing process, the Ar-PBS-Ar sample was similar to the ordinary silk with addition flame retardant property.

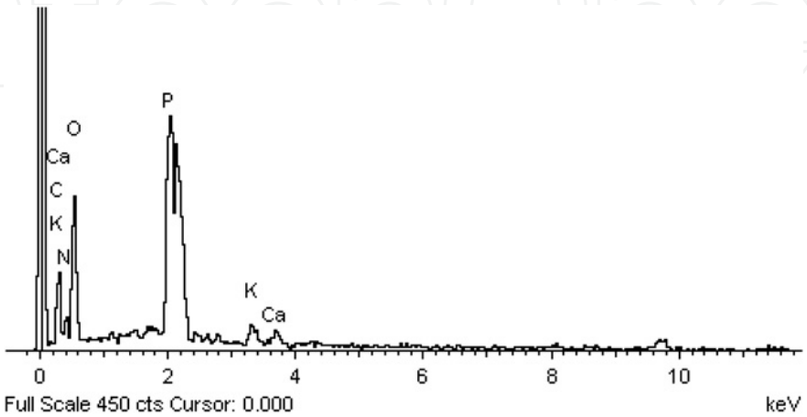

Fig. 8. The EDS spectrum of washed Ar-PBS-Ar silk (Au peak was not subtracted.).

The washed Ar-PBS-Ar silk sample has been characterized by ATR-FTIR in comparison with the untreated as shown in Fig. 9. Graft-polymerization via Ar plasma was indicated by the presence of bands at 1196 cm^{-1} (C–O stretching vibration), 1078 cm^{-1} and 919 cm^{-1} (P–O–C stretching vibration). The P═O stretching vibration that indicates the PBS compound overlapped within the C–O band. The IR peak intensity changes seem relatively low indicated the very thin layer of graft-PBS on silk surface from plasma treatment.

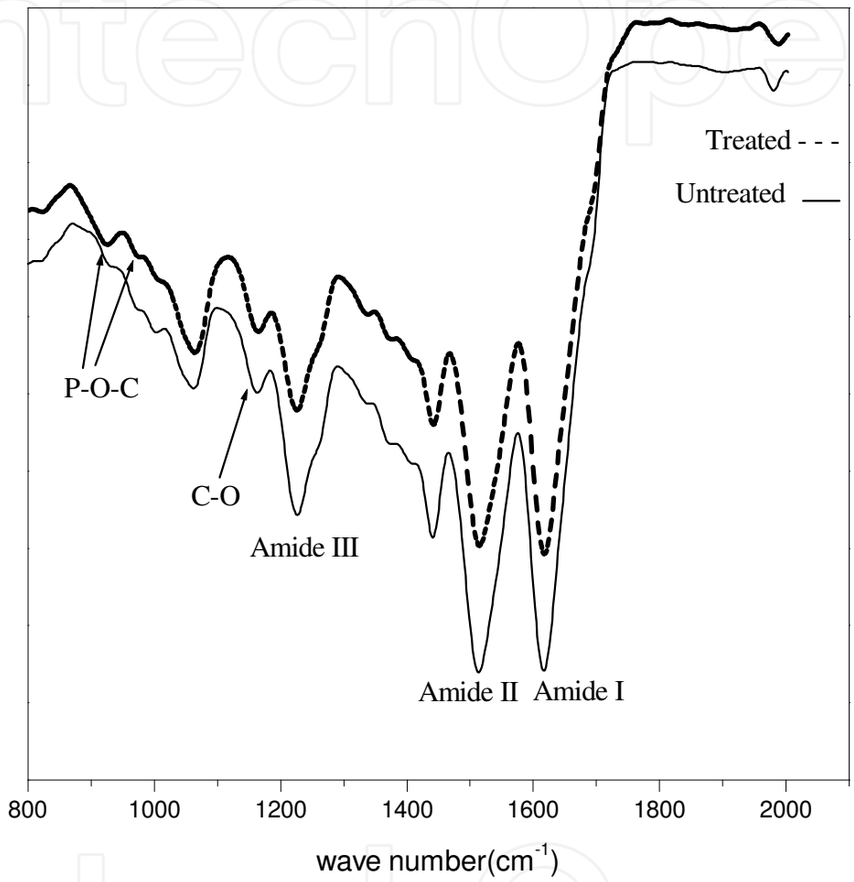

Fig. 9. ATR-FTIR spectra of untreated and washed Ar-PBS-Ar silk.

2.6.3 Flame retardancy testing

Burning behavior and 45-degree flame spread rate of untreated and treated cotton fabrics before and after washing were examined using 45° Flammability Tester according to ASTM D1230 with the impingement time of 5 sec at 30°C and 62 +/- 3% RH. The burning behavior and flame spread was recorded by a digital video camera. The flame spread time is the time taken for any flaming to proceed a distance of 12.7 cm (5″) up the fabric, and is automatically recorded by the burning of a stop cord. Fig. 10 shows the burning behavior of the silk samples. The samples prepared with different procedures were tested. In the case of untreated silk, the sample ignited instantly with a rapid flame spread of 1.43 cm/s. The flame extended to the entire sample without burning smoke. For the sample directly

(a)

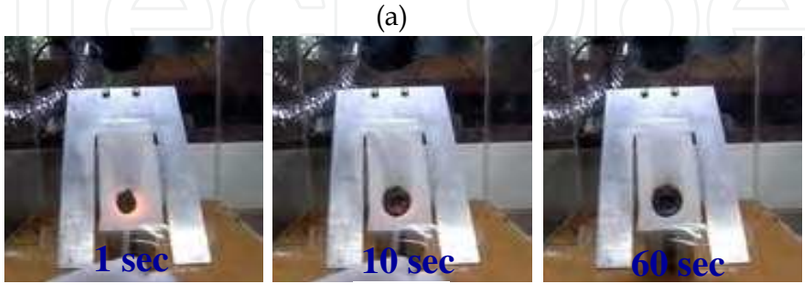

(b)

(c)

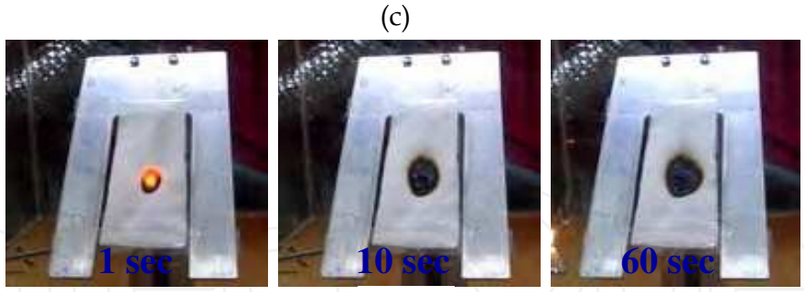

(d)

Fig. 10. Burning behavior of; a) untreated silk, completely burned within 7 s; b) PBS silk; c) washed Ar-PBS-Ar silk and; d) ethanol wash only.

immersed in PBS solution (PBS silk), the ignition character was identical to that of the untreated sample but the flame spread terminated immediately. The sample did not exhibit the afterglow. Burning smoke, as a consequence of char formation, was observed. The char formation is an indication of phosphorus containing residue on the surface of the sample (Tsafack & Levalois-Grützmacher, 2006a). The compound decomposed to polyphosphoric acid when heated and formed a viscous surface layer. This layer prevents oxygen to reach the silk fiber. As a consequence the fiber decomposition is inhibited.

After the washing process the burning behavior of the PBS silk was similar to that of the untreated sample. Some burning smoke was observed. This is due to the fact that PBS is water soluble, thus it can be removed from the silk during washing process. The smoke indicated that some PBS remained in the silk. In contrast, the Ar-PBS-Ar silk behaved differently. Its flame spread was higher than the PBS sample. However, the flame vanished immediately without the afterglow. The char formation was observed. This small amount of phosphorus catalyzes the oxidation of the carbon char to carbon monoxide instead of carbon dioxide during pyrolysis. The burning smoke was dramatically reduced to the amount that is close to the untreated sample. Since burning smoke mainly comes from the residual PBS on the surface of the sample, it can be said that most of the PBS molecules were grafted homogeneously into the silk molecular chains by the Ar plasma. Washing process might take away the un-grafted PBS molecules from the silk structure but the majority remained intact in the silk structure. Hence, with adequate level of grafted PBS molecules, silk samples can generate char to prevent flame spread without excess burning smoke.

2.7 The simulation

Molecular dynamic (MD) simulation of silk structure

To study the chemical bonding between PBS and the silk structure, MD simulation was performed. The simulation to predict the IR spectrum of silk after the incorporation of PBS was carried out to envisage the interactions. Silk model was generated using repeating glycine–alanine unit as discussed in the previous study (Khomhoi *et al.* 2010). Material Studio 4.3 software was used to build the model and perform energy minimization and MD simulations of the macroscopic structure of silk polymer containing 5 chains of 10-unit glycine–alanine in a periodic box of 30 × 30 × 30 Å using COMPASS forced field. Energy minimization was carried out to eliminate the potential energy which might arise as a result of the interaction with the neighboring chains with conjugate gradient method. After the minimized cell was obtained, the simulated annealing with Metropolis Monte Carlo (MC) method of Sorption module was designed to simulate the interaction between PBS and the silk model. The cut off distance was set at 12.5 Å for micro canonical ensemble. Trajectories from the MC simulation were collected for radial distribution analysis. To predict the IR spectrum of silk after plasma treatment process, quantum calculation of silk model compound modified by PBS predicted product from MD simulation was performed using GAUSSIAN 03 (Frisch *et al.* 2004). B3LYP/6-31G (d) level of density functional theory (DFT) was used to calculate optimized structure and IR frequencies.

The interactions between PBS and silk was investigated through MC simulation using model shown in Fig. 11. The most probable structure from MC simulation indicated that the reactive oxygen atom in P═O and P–O–N part of PBS molecule tend to react with silk polymer surface at methyl group of alanine unit.

The radial distribution function (RDF) plot (Fig. 12) of H_{meth}–$O_{O=P}$ and H_{meth}–O_{P-O-N} represent P═O and P–O–N in PBS surrounding methyl group in silk. RDF calculated from collected trajectories suggest that the distribution of PBS around silk was contributed from strong interaction of P═O and P–O–N in PBS with methyl group in silk. The graph infers that H_{meth}–$O_{O=P}$ dominate intermolecular interaction in term of hydrogen bonding from strongest electrostatic interaction of partial negative oxygen and partial positive hydrogen with shell of interaction at 3.25 Å. On the other hand, H_{meth}–O_{P-O-N}interaction is mostly

diffuse with radius around 4–9 Å. Therefore P═O group of PBS should react with methyl group of alanine residue in silk.

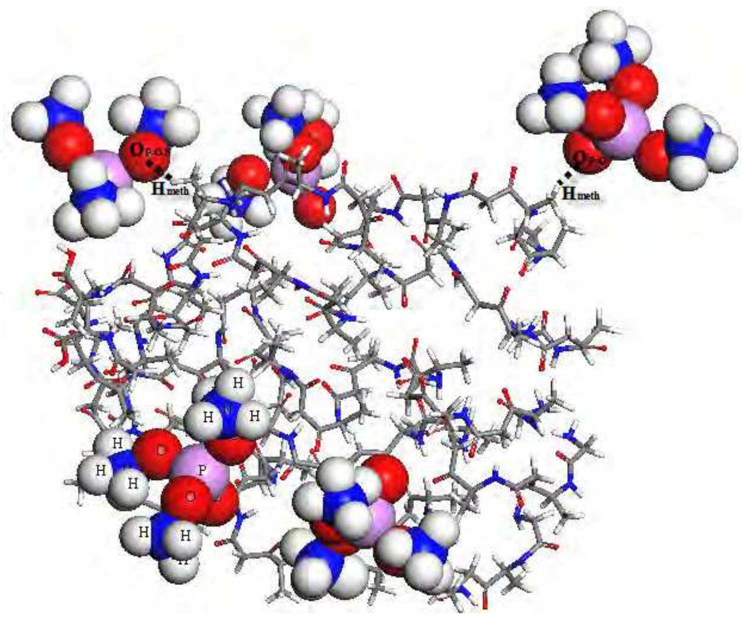

Fig. 11. Complex structure of silk model and PBS molecules system from Monte Carlo Simulated Annealing, dash line indicate strong interaction of P═O and P–O–N in PBS with methyl group in silk at distance 2.50–2.60 Å.

Product of PBS reacting with silk was deduced using above mentioned evident as shown in Fig. 13 in comparison with silk model. The use of calculations level at B3LYP/6-31G(d) show C═O stretching at 1777 and 1844 cm^{-1}, the stretching of C–O bond presents at 1196 cm^{-1} while group of N–H bending and C–N stretching was found in range of 1200–1700 cm^{-1} for both untreated and PBS silk. The P–O–C stretching vibration at 1078 cm^{-1} and medium peak of P–O–C stretching vibration at 919 cm^{-1} were found correlated well with previous studies (Zanini *et al.* 2008) and (Zou *et al.* 2002).

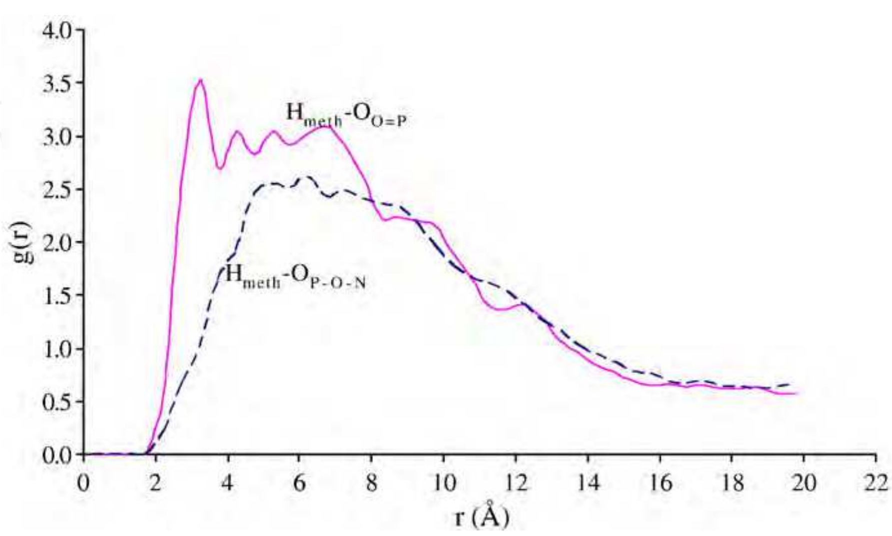

Fig. 12. Radial distribution function of H_{meth}–$O_{O=P}$ and H_{meth}–O_{P-O-N} represent P=O and P–O–N in PBS surrounding methyl group in silk.

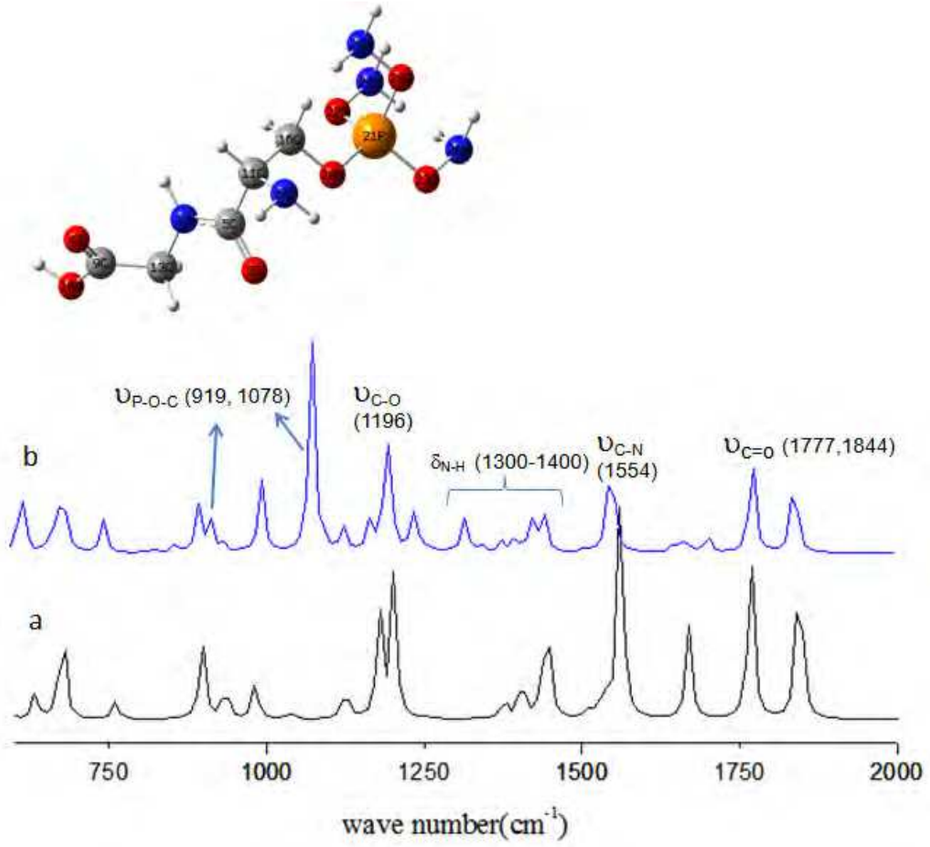

Fig. 13. Vibration spectrum of silk and propose product after treated structure calculated by using B3LYP/6-31G(d); a) untreated silk and; b) PBS silk.

3. Conclusions

Non-equilibrium atmospheric plasma jet has been proved for its benefit on high-density active species generation, low gas-surface temperature, direct treatment and low cost system. The reactive species in the plasma interact with the surface atoms or molecules and modify the surface without affecting bulk properties. Also penetration of jet plasma into woven materials such as textile fabrics can be achieved. This near-room temperature modification makes plasma jet of industrial interests. Phosphorus-based flame retardants becomes a major source of interest to replace halogen compounds because of their environmentally friendly by-products and their low toxicity.

The graft polymerization was needed because of phosphorus-based flame retardant agent is non-durable to washing. Plasma jet with selective ions can be used to replace chemical agent(s) with time-consuming pad-dry processes. The flame retardant property of silk fabrics induced by grafting of flame retardant compound using Ar plasma jet has been investigated. It has been shown that Ar plasma grafting is a necessary procedure to achieve the durable flame retardant property. Ar plasma grafting conferred endurable flame retardant property to silk fabric. The good washing stability could be attributed to the presence of phosphorus that was covalently bound to the silk structure.

The Ar-grafted PBS silk showed a higher level of flame retardancy as investigated by burning behavior and 45^{o} flammability test. Carbonaceous char was formed and after glow was suppressed by PBS grafting. It was found that Ar plasma conferred durable flame retardancy to the silk yarn since the flame retardant character retained to washing. In the study, the Ar-grafted PBS silk improved the durability of the flame retardancy by decreasing 45-degree flame spread rate about 9.5 times. Also their low production of smoke in fire furthers their appeal. These compounds promote dehydration and char formation on their substrate preventing flame spread. Scanning electron microscopy results illustrated that the yarn of the Ar-grafted silk was uniformly covered with the PBS particles whereas PBS deposited locally on the non-graft silk. Energy dispersive X-ray spectroscopy showed the presence of phosphorus up to 11 wt.% in the Ar-grafted silk. Fourier transform infrared spectroscopy exhibited the bondings between phosphorus and the silk molecular chains. The molecular dynamics simulations affirmed the incorporation of phosphorus in the structure of silk at methyl group of alanine unit since the predicted IR spectrum agree well with the measured one.

4. Acknowledgment

DB would like to thank Chiang Mai University for research funding and laboratory supports. Thanks and appreciations also go to colleagues and students in the project and people who have willingly helped me out with their abilities.

5. References

Achwal, W.B. Mahapatrao, C.R. and Kaduska, P.S. (1987) *Colourage* 6, p. 16.

Becker, K.H. Kogelschatz, U. Schoenbach, K. H. Barker, R.J.(2004) *Non-equilibrium air plasmas at atmospheric pressure; Series in Plasma Physics*, Taylor & Francis: New York

Chaiwong, C. Tunma, S. Sangprasert, W. Nimmanpipug, P. Boonyawan, D. (2010) *Surf. Coat. Technol.* 204, p. 2991.

Cheng, C. Liye, Z. and Zhan, R.-J.(2006) *Surf. Coat. Technol.* 200, p. 6659

Coburn, J.W. and Winters, H.F. (1979) *J. Appl. Phys.*, *50*(5) p. 3189

Dhavalaikar, R.S. (1962) *J. Scientific and Industrial Res.* 21(C), p. 261

Fridman, A. (2008) *Plasma Chemistry*; Cambridge University Press: New York

Frisch, M. J. Trucks, G. W. Schlegel, H. B. Scuseria, G. E. Robb, M. A. Cheeseman, J. R. Montgomery, Jr., J. A. Vreven, T. Kudin, K. N. Burant, J. C. Millam, J. M. Iyengar, S. S. Tomasi, J. Barone, V. Mennucci, B. Cossi, M. Scalmani, G. Rega, N. Petersson, G. A. Nakatsuji, H. Hada, M. Ehara, M. Toyota, K. Fukuda, R. Hasegawa, J. Ishida, M. Nakajima, T. Honda, Y. Kitao, O. Nakai, H. Klene, M. Li, X. Knox, J. E. Hratchian, H. P. Cross, J. B. Bakken, V. Adamo, C. Jaramillo, J. Gomperts, R. Stratmann, R. E. Yazyev, O. Austin, A. J. Cammi, R. Pomelli, C. Ochterski, J. W. Ayala, P. Y. Morokuma, K. Voth, G. A. Salvador, P. Dannenberg, J. J. Zakrzewski, V. G. Dapprich, S. Daniels, A. D. Strain, M. C. Farkas, O. Malick, D. K. Rabuck, A. D. Raghavachari, K. Foresman, J. B. Ortiz, J. V. Cui, Q. Baboul, A. G. Clifford, S. Cioslowski, J. Stefanov, B. B. Liu, G. Liashenko, A. Piskorz, P. Komaromi, I. Martin, R. L. Fox, D. J. Keith, T. Al-Laham, M. A. Peng, C. Y. Nanayakkara, A.; Challacombe, M. Gill, P. M. W. Johnson, B. Chen, W. Wong, M. W. Gonzalez, C. and Pople, J. A. (2004) *Gaussian 03, Revision C.02,* Gaussian, Inc., Wallingford, CT.

Gaan, S. and Sun, G. *J.* (2007) *Anal. Appl. Pyrol.* 78 , p. 371.
Griem, H.R. (1964) *Plasma Spectroscopy.* McGraw-Hill, New York
Grill, A. (1994) *Cold Plasma Materials Fabrication: From Fundamentals to Applications*; Wiley-IEEE Press: New York
Grzegorzewski, F. (2011) *PhD. Dissertation*, University of Berlin, p. 29
Guan, J. and Chen, G.Q. (2006) *Fire Mater.* 30, p. 415.
Guan, J. Yang, C.Q. and Chen, G. (2009) *Polym. Degrad. Stabil.* 94, p. 450.
Guimin, X. Guanjun, Z. Xingmin, S. Yue, M. Ning, W. and Yuan, L. (2009) *Plasma Sci. Technol.* 83.
Horrocks, A.R. and Price, D. (2001) *Camb. Woodh. Publ. Limit.* ISBN:1855734192.
Kako, T. and Katayama, A. (1995) *Nippon Sanshigakul Zasshi.* 64, p. 124.
Khomhoi, P. Sangprasert, W. Lee, V.S. Nimmanpipug, P. (2010) *Chiang Mai J. Sci.* 37 (1) 106.
Kurunczi, P. Lopez, J. Shah, H. Becker, K. (2001) *Int. J. Mass Spec., 205*(1-3), 277
Kylian, O. Benedikt, J. Sirghi, L. Reuter, R. Rauscher, H. Von Keudell, A. Rossi, F. (2009) *Plasma Process. Polym. 6*, p.255.
Mathew, T. Datta, R.N. Dierkes, W.K. Noordermeer, J.W.M. Van Ooij, Mechanistic, W.J. (2008) *Plasma Chem. Plasma Proc. 28*, 273.
Naganathan, P.S. and Venkatesan, K. (1972) *Acta Crystallographica Section B* 28, p. 552
Osaki, K. Fujimoto, S. and Fukumasa, O. (2003) *Thin Solid Films Proceedings of the Joint International Plasma Symposium of the 6th APCPST, the 15th SPSM and the 11th Kapra Symposia* vol. 435, p. 56.
Raballand, V. Benedikt, J. Wunderlich, J. Von Keudell, A. (2008) *J. Phys. D: Appl. Phys.* 41, p.115207.
Reddy, P.R.S. Agathian, G. and Kumar, A. (2005) *Radiat. Phys. Chem.* 72, p. 511.
Sangprasert W., Boonyawan D. and Nimmanpipug P. (2010). *Journal of Molecular Structure*, 963 (2-3) 130-136
Schafer, J. Foest, R. Quade, A. Ohl, A. and Weltmann, K.-D. (2008) *J. Appl. Phys.* 194010.
Sismanoglu, B. N. Amorim, J. A Souza-Corrêa, A. Oliveira, C. Gomes, M.P. (2009) *Spectrochimica Acta Part B* 64, 1287-1293
Takahashi, Y. Gehoh, M. And Yuzuriha, K. (1999) *Int. J. Biological Molecules* 24, p.127
Tanter, T.C. (1953) *Acta Crystallographica Section B* 26, p. 805
Tanter, T.C. (1956) *Nature* 177, p. 37
Tsafack, M.J. and Levalois-Grützmacher, (2006) J. *Surf. Coat. Technol.* 201, p. 2599.
Tsafack, M.J. and Levalois-Grützmacher, J. (2006a) *Surf. Coat. Technol.* 200, p. 3503.
Von Keudell, A. and Jacob, W. (2004) *Prog. Surf. Sci.* 76, p.21
Wichman, I.S. (2003) *Prog. Energ. Combust.* 29, p. 247.
Wu, W. and Yang, C.Q. (2006) *Polym. Degrad. Stabil.* 91 , p. 2541
Wu, W. and Yang, C.Q. (2007) *Polym. Degrad. Stabil.* 92, p. 363.
www.NIST.gov (2009) accessed via internet
Yang, H. and Yang, C.Q., (2005) *Polym. Degrad. Stabil.* 88, p. 363.
Zanini, S. Riccardi, C. Orlandi, M. Colombo, C. and Croccolo, F. (2008) *Polym. Degrad Stabil.* 93, p. 1158.
Zou, X.P. Kang, E.T. and Neoh, K.G. (2002) *Surf. Coat. Technol.* 149, p.119.

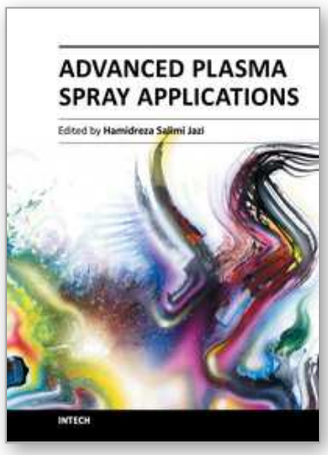

Advanced Plasma Spray Applications
Edited by Dr. Hamid Jazi

ISBN 978-953-51-0349-3
Hard cover, 250 pages
Publisher InTech
Published online 21, March, 2012
Published in print edition March, 2012

Recently, plasma spray has been received a large number of attentions for various type of applications due to the nature of the plasma plume and deposition structure. The plasma gas generated by the arc, consists of free electrons, ionized atoms, some neutral atoms, and undissociated diatomic molecules. The temperature of the core of the plasma jet may exceed up to 30,000 K. Gas velocity in the plasma spray torch can be varied from subsonic to supersonic using converging-diverging nozzles. Heat transfer in the plasma jet is primarily the result of the recombination of the ions and re-association of atoms in diatomic gases on the powder surfaces and absorption of radiation. Taking advantages of the plasma plume atmosphere, plasma spray can be used for surface modification and treatment, especially for activation of polymer surfaces. I addition, plasma spray can be used to deposit nanostructures as well as advanced coating structures for new applications in wear and corrosion resistance. Some state-of-the-art studies of advanced applications of plasma spraying such as nanostructure coatings, surface modifications, biomaterial deposition, and anti wear and corrosion coatings are presented in this book.

INTECH
open science | open minds

InTech Europe
University Campus STeP Ri
Slavka Krautzeka 83/A
51000 Rijeka, Croatia
Phone: +385 (51) 770 447
Fax: +385 (51) 686 166
www.intechopen.com

InTech China
Unit 405, Office Block, Hotel Equatorial Shanghai
No.65, Yan An Road (West), Shanghai, 200040, China
中国上海市延安西路65号上海国际贵都大饭店办公楼405单元
Phone: +86-21-62489820
Fax: +86-21-62489821

IntechOpen